Electronic Supplementary Information

Homogeneous Localized Surface Plasmon Resonance Inflection Points for Enhanced Sensitivity and Tracking Plasmon Damping in Single Gold Bipyramids

Philippe Vuka Tsalu, Geun Wan Kim, Jong Wook Hong, and Ji Won Ha*

Department of Chemistry, University of Ulsan, 93 Daehak-Ro, Nam-Gu, Ulsan 44610, South Korea

*To whom correspondence should be addressed.

J. W. Ha

Phone: +82-52-712-8012

Fax: +82-52-712-8002

E-mail: jwha77@ulsan.ac.kr

<Table of Contents>

1. **Electrodynamics for Gold Bipyramids and LSPR Inflection Points**
2. **Changes of the Complex Dielectric Functions**
3. **Noise Analysis**
4. **Effect of Substrate on Scattering Properties of Single AuBPs**
5. **References**
6. **Supplementary Tables (Table S1 to S4)**
7. **Supplementary Figures (Fig. S1 to S7)**

1. Electrodynamic for Gold Bipyramids and LSPR Inflection Points

For nanoparticles the optical cross sections as a function of energy are dominated by the localized surface plasmon resonance[1]. At the resonance energy (or wavelength), the peak position and linewidth are determined by the size and shape of nanoparticle as well as the dielectric surrounding environment. By solving Maxwell's equations using Mie theory and considering only the lowest dipolar mode (dipolar approximation) the scattering cross section solution can varies for different shapes of nanoparticles characterized by a frequency-dependent complex dielectric function $\varepsilon_{1(\omega)} + \varepsilon_{2(\omega)}$ embedded in a medium of dielectric $\varepsilon_m = n_m^2$.[1-2] For an ellipsoid (such as bipyramids) along one of its main axis, the extinction cross section in the dipolar approximation is well described by the analytical expression given by the equation (1)[3]:

$$\sigma_{ext}(\lambda) = \frac{2\pi V \eta_m^3}{\lambda \beta^2} \frac{\varepsilon_2(\lambda)}{\left| \varepsilon(\lambda) + \frac{1-\beta}{\beta} \eta_m^2 \right|^2} \quad (1)$$

where β is a shape-dependent factor (only depend on the aspect ratio for nano-spheroid). For a weakly dispersed $\varepsilon_{2(\lambda)}$ around the LSPR peak maximum (λ_{res}) (e.g., away from the inter-band absorption), the resonance condition is well approximated by $\varepsilon_1(\lambda_{res.}) \approx (\beta - 1)\eta_m^2 / \beta$. The LSPR width can then be estimated developing equation (1) around the LSPR frequency[3-4] ω_{res} to obtain equation (2):

$$\sigma_{ext}(\lambda) = \frac{\omega V \eta_m^3}{2c\beta^2 \left(\partial\varepsilon_1 / \partial\omega \right)_{\omega_{res.}}} \frac{\Gamma}{(\omega - \omega_{res.})^2 + (\Gamma/2)^2} \quad (2)$$

With the angular frequency $\omega=(2\pi c/\lambda)$. The LSPR thus exhibits a quasi-Lorentzian profile[1, 3] with a full width at half maximum (FWHM) Γ that took the same form as in gold bipyramids from our results and given by the Lorentzian fitting curves:

$$I_{Scat.} = I_0 + \left(\frac{2A}{\pi}\right)\frac{\Gamma}{4\left(\omega-\omega_{res.}\right)^2+\Gamma^2} \quad (3)$$

Where I_o and A are offset and area under the peak respectively. In a nano-sphere under the same approximations[4]:

$$\Gamma = 2\varepsilon_2\left(\omega_{res.}\right) \Big/ \left(\partial\varepsilon_1 \Big/ \partial\omega\right)_{\omega_{res.}} \quad (4)$$

The LSPR scattering spectra were fitted with the use of a Lorentzian function depicted by equation (3) to determine the LSPR linewidth Γ and the resonance frequency ω_{res}. First and second order derivatives of the LSPR scattering spectra were performed by the use of equations (5) and (6), respectively.

$$\frac{dI_{Scat.}}{d\omega} = -\left(\frac{16A}{\pi}\right)\frac{\left(\omega-\omega_{res.}\right)\omega}{\left[4\left(\omega-\omega_{res.}\right)^2+\Gamma^2\right]^2} \quad (5)$$

$$\frac{d^2I_{Scat.}}{d\omega^2} = -\left(\frac{16A}{\pi}\right)\frac{\left[\Gamma^2-12\left(\omega-\omega_{res.}\right)^2\right]\omega}{\left[4\left(\omega-\omega_{res.}\right)^2+\Gamma^2\right]^3} \quad (6)$$

For every first and second derivation, the local maximum/maximum and inflection points were extracted for peak energies analysis. The FWHM obtained between the two inflection points were in good agreement with that of equation (3).

2. Changes of the Complex Dielectric Functions

The changes in the complex dielectric functions in the vicinity of single gold bipyramids embedded local RI media used in this work is introduced by considering Kramers-Kronig consistent Lorentz transformations[5]. In the light absorption and scattering by small particles experiments, the real and imaginary parts of optical properties that are frequency-dependent complex functions of the driving electric field such as polarizability[6], dielectric[7] and refractive index[8] are related. For instance, in the positives frequencies ranges, the changes of real and imaginary parts of complex polarizability functons can be break down in equations (7) and (8) expressed by dispersion relations[9], and are called Kramers-Kronig transformations[5].

$$\chi_r(\omega) = \frac{2}{\pi} P\int_0^{\infty} \frac{\Omega \chi_i(\omega)}{\Omega^2 - \omega^2} d\Omega \quad (7)$$

$$\chi_i(\omega) = -\frac{2\omega}{\pi} P\int_0^{\infty} \frac{\Omega \chi_r(\omega)}{\Omega^2 - \omega^2} d\Omega \quad (8)$$

Where χ_i, χ_r, ω, Ω and P indicate the frequency-dependent imaginary part, the frequency-dependent real part, the angular frequency ($2\pi c/\lambda$), a parameter related to the change in the absorption coefficient[8] and the principal value of the integral, respectively. The frequency-dependent real and imaginary parts are connected by integrations. This analytic property imposes a constraint on physically realizable susceptibility/polarizabilities or others optical responses, since the optical constants must satisfy Kramers-Kronig relation[10] (or dispersion relations) to be physical[11]. In this relation, if the frequency-dependent real part is known over a sufficiently large range of angular frequencies ω, the frequency-dependent imaginary part can be obtained by integration, and vice versa, that is, one is the derivative of another[12]. The change of analytic relative frequency-dependent complex dielectric function is then obtained by $\overset{\circ}{\varepsilon}_r = 1 + \chi$ and

integrals in equations (7) and (8) relate area under the frequency-dependent imaginary part of the complex dielectric or susceptibility/polarizability functions to shape of frequency-dependent real part of the complex dielectric and vice-versa[13]. From the same theory (S1) it was inferred from the Lorentzian form of both, scattering cross section and absorption cross section that the real part of the dielectric function determines the plasmon resonance position whereas the imaginary part governs the linewidth[1]. Therefore, using this dipole approximation equation, we derived both the real and imaginary part. Indeed, in analyzing the shift of the plasma resonance in the optical properties for small metal particles[1414145], L. Genzel and T.P Martin used the changes of frequency-dependent complex dielectric functions in the local neighborhood of small metal particle exhibiting a uniform mode plasmon resonance an given by the classical dipole approximation through the one single Lorentzian oscillator dipole functions[1, 151, 151, 151, 6], which analytically is given in equation (9) as a photon energy function.

$$\overset{\circ}{\varepsilon}_r(E) = 1 - \sum_j \frac{A_j}{{E_0}^2{}_j - E^2 + i\Gamma_j E} \quad (9)$$

Where A_j, E_o, E and, Γ denote oscillator strength, resonance photon energy, photon energy and damping coefficient, respectively. The complex dielectric is described as sum of different oscillators and the subscript j depicts the jth oscillator. The energy-dependent imaginary part form of equation (3) is often referred to as Lorentzian. Fundamentally, the Lorentz model assumes a physical model in which the electron oscillates in viscous fluid[15] and account the inter-band transition contributions. The phase and amplitude of electric dipole are obtained by equation (10) and (c), respectively:

$$\delta_{dip} = \tan^{-1}\left(-\frac{\Gamma E}{{E_0}^2 - E^2}\right) \quad (10)$$

The amplitude of electric dipole:

$$a_{dip} = \frac{1}{\left[\left(E_0{}^2 - E^2\right)^2 - \Gamma^2 E^2\right]^{\frac{1}{2}}} \quad (11)$$

Approximately for the scattering first and second derivatives, the oscillator phases of electric dipole were obtained by equation (d):

$$\delta_{dip} = \tan^{-1}\left[-\frac{\mathrm{Im}[\varepsilon(\omega)]}{\mathrm{Re}[\varepsilon(\omega)]}\right] \approx \tan^{-1}\left[\frac{\frac{dI_{scat.}}{d\omega}}{I_{scat}}\right] \quad (12)$$

The LSPR quality factor is obtained by the equation (13)

$$Q_{LSPR} = \frac{\left|\mathrm{Re}[\varepsilon(E)]\right|}{\mathrm{Im}[\varepsilon(E)]} \quad (13)$$

The second member of equation (12) is the phase-like in terms or derivations for Lorentzian-like signal.

3. Noise Analysis

Unfortunately, noise-free data can never be realized in laboratory because some types of noise arise from thermodynamic and quantum effects that are impossible to avoid in a measurement[16]. In traditional LSPR based sensing experiment, monitoring shifts of the peak position in response to local refractive index (RI) changes is limited by instrumental and chemical noise, due to the limited ability of resolving minute shifts changes in the LSPR position peak and shape, so-called broadening and asymmetry. Noise associated with our experiment data, especially the LSPR scattering peak maxima depicted by capital B (Fig. 2A, the first line), inflexion points A and C in the local air, water and oil RI media. As it can be seen from the tables S1 and S2 the method did not propagate the noise significantly.

4. Effect of Substrate on Scattering Properties of Single AuBPs

The dielectric properties of substrates such as silicon and gold can change the scattering features of single AuBPs. In other words, the substrate where AuBPs are deposited can strongly influence their plasmon resonance frequencies and spectral line-shapes.[17-18] For example, the LSPR of 60-nm gold nanospheres in a uniform dielectric medium of air has a peak at 535 nm; in contrast, when the same nanosphere is placed on a gold film (~50 nm thick), the SPR peak is dramatically red-shifted to ~655 nm.[19] This spectral shift is consistent with the interaction between two closely spaced nanoparticles with the incident electric field polarized parallel to the line connecting the nanoparticle centers. Furthermore, as another example, the scattering pattern appears as a solid bright spot (Figure 1B) when gold nanorod (AuNR) is deposited on a glass slide, or a doughnut shape when the AuNR is deposited on a gold film.[17]

In the present study, we used a glass slide as the substrate for investigating the scattering properties of single AuBPs. Therefore, we measured all of single AuBPs deposited on the glass substrate and successfully demonstrated the enhanced RI sensitivity using the LSPR IFs over their counterpart LSPR peak shift locations. The results of this investigation support the idea that tracking curvature changes of an optical signal can be effectively used for LSPR longitudinal peak RI sensing as well as damping in the local RI environment of a single AuBP.

5. References

[1] Olson, J.; Dominguez-Medina, S.; Hoggard, A.; Wang, L.-Y.; Chang, W.-S.; Link, S., Optical Characterization of Single Plasmonic Nanoparticles. *Chemical Society reviews* **2015,** *44* (1), 40-57.

[2] Amendola, V.; Pilot, R.; Frasconi, M.; Marago, O. M.; Iati, M. A., Surface plasmon resonance in gold nanoparticles: a review. *J Phys Condens Matter* **2017,** *29* (20), 203002.

[3] Lombardi, A.; Loumaigne, M.; Crut, A.; Maioli, P.; Del Fatti, N.; Vallee, F.; Spuch-Calvar, M.; Burgin, J.; Majimel, J.; Treguer-Delapierre, M., Surface plasmon resonance properties of single elongated nano-objects: gold nanobipyramids and nanorods. *Langmuir : the ACS journal of surfaces and colloids* **2012,** *28* (24), 9027-33.

[4] Baida, H.; Billaud, P.; Marhaba, S.; Christofilos, D.; Cottancin, E.; Crut, A.; Lerme, J.; Maioli, P.; Pellarin, M.; Broyer, M.; Del Fatti, N.; Vallee, F.; Sanchez-Iglesias, A.; Pastoriza-Santos, I.; Liz-Marzan, L. M., Quantitative determination of the size dependence of surface plasmon resonance damping in single Ag@SiO(2) nanoparticles. *Nano letters* **2009,** *9* (10), 3463-9.

[5] Polavarapu, P. L., Kramers-Kronig transformation for optical rotatory dispersion studies. *The journal of physical chemistry. A* **2005,** *109* (32), 7013-23.

[6] Keefe, C. D., Curvefitting Imaginary Components of Optical Properties: Restrictions on the Lineshape Due to Causality. *Journal of Molecular Spectroscopy* **2001,** *205* (2), 261-268.

[7] Dressel, M.; Gompf, B.; Faltermeier, D.; Tripathi, A. K.; Pflaum, J.; Schubert, M., Kramers-Kronig-consistent optical functions of anisotropic crystals: generalized spectroscopic ellipsometry on pentacene. *Opt. Express* **2008,** *16* (24), 19770-19778.

[8] Haes, A. J.; Zou, S.; Zhao, J.; Schatz, G. C.; Van Duyne, R. P., Localized surface plasmon resonance spectroscopy near molecular resonances. *J Am Chem Soc* **2006,** *128* (33), 10905-14.

[9] Polavarapu, P. L.; Petrovic, A. G.; Zhang, P., Kramers-Kronig transformation of experimental electronic circular dichroism: application to the analysis of optical rotatory dispersion in dimethyl-L-tartrate. *Chirality* **2006,** *18* (9), 723-32.

[10] Hall, S. H.; Heck, H. L., *Advanced Signal Integrity for High-Speed Digital Designs*. Wiley-IEEE Press: 2009; p 660.

[11] Akyurtlu, A.; Kussow, A.-G., *Relationship between the Kramers-Kronig relations and negative index of refraction*. 2010; Vol. 82.

[12] Gorkunov, M. V.; Dmitrienko, V. E.; Ezhov, A. A.; Artemov, V. V.; Rogov, O. Y., Implications of the causality principle for ultra chiral metamaterials. *Scientific Reports* **2015,** *5*, 9273.

[13] Lovell, R., Application of Kramers-Kronig relations to the interpretation of dielectric data. *Journal of Physics C: Solid State Physics* **1974,** *7* (23), 4378.

[14] Genzel, L.; Martin, T. P.; Kreibig, U., Dielectric function and plasma resonances of small metal particles. *Zeitschrift für Physik B Condensed Matter* **1975,** *21* (4), 339-346.

[15] Bohren, C. F.; Huffman, D. R., Absorption and Scattering by an Arbitrary Particle. In *Absorption and Scattering of Light by Small Particles*, Wiley-VCH Verlag GmbH: 2007; pp 57-81.

[16] Skoog, D. A.; Crouch, S. R.; Holler, F. J., *Principles of instrumental analysis*. Thomson Brooks/Cole: Belmont, CA, 2007.

[17] Chen, H.; Ming, T.; Zhang, S.; Jin, Z.; Yang, B.; Wang, J., Effect of the Dielectric Properties of Substrates on the Scattering Patterns of Gold Nanorods. *ACS Nano* **2011,** *5* (6), 4865-4877.

[18] Ha, J. W.; Marchuk, K.; Fang, N., Focused Orientation and Position Imaging (FOPI) of Single Anisotropic Plasmonic Nanoparticles by Total Internal Reflection Scattering Microscopy. *Nano Letters* **2012,** *12* (8), 4282-4288.

[19] Mock, J. J.; Mock, J. J.; Hill, R. T.; Degiron, A.; Zauscher, S.; Chilkoti, A.; Smith, D. R. *Nano Lett.* **2008**, *8*, 2245–2252.

6. Supplementary Tables

Single AuBPs	1	2	3	4	5	6	7	8	9	10	Ave.	Std.
Inflection A (eV)	1.72	1.80	1.69	1.79	1.85	1.74	1.80	1.83	1.74	1.82	1.78	0.05
LSPR B (eV)	1.76	1.84	1.74	1.84	1.90	1.78	1.84	1.87	1.78	1.86	1.82	0.05
Inflection C (eV)	1.79	1.88	1.78	1.89	1.95	1.82	1.88	1.91	1.82	1.90	1.86	0.06

Table S1. Inflection points and LSPR locations on the curvatures in refractive index of air

Single AuBPs	1	2	3	4	5	6	7	8	9	10	Ave.	Std.
Inflection A (eV)	1.68	1.63	1.61	1.66	1.72	1.67	1.66	1.65	1.64	1.64	1.66	0.03
LSPR B (eV)	1.72	1.66	1.67	1.69	1.77	1.70	1.69	1.68	1.68	1.67	1.69	0.03
Inflection C (eV)	1.75	1.70	1.73	1.72	1.81	1.74	1.73	1.72	1.71	1.71	1.73	0.03

Table S2. Inflection points and LSPR locations on the curvatures in refractive index of water

Single AuBPs	1	2	3	4	5	6	7	8	9	10	Ave.	Std.
Inflection A (eV)	1.54	1.57	1.47	1.57	1.54	1.54	1.56	1.55	1.55	1.58	1.55	0.03
LSPR B (eV)	1.56	1.60	1.50	1.60	1.57	1.57	1.59	1.58	1.58	1.61	1.58	0.03
Inflection C (eV)	1.59	1.63	1.53	1.63	1.60	1.60	1.62	1.62	1.60	1.64	1.61	0.03

Table S3. Inflection points and LSPR locations on the curvatures in refractive index of oil

Single AuBPs	1	2	3	4	5	6	7	8	9	10	Ave.	Std.
Slope at Inflection A ($eV \cdot RIU^{-1}$)	0.32	0.45	0.41	0.42	0.58	0.37	0.46	0.54	0.36	0.48	0.44	0.080
Slope at LSPR B ($eV \cdot RIU^{-1}$)	0.36	0.48	0.44	0.47	0.61	0.39	0.48	0.56	0.38	0.50	0.47	0.080
Slope at Inflection C ($eV \cdot RIU^{-1}$)	0.36	0.49	0.45	0.51	0.65	0.41	0.50	0.56	0.42	0.51	0.49	0.080

Table S4. Sensitivities

7. Supplementary Figures

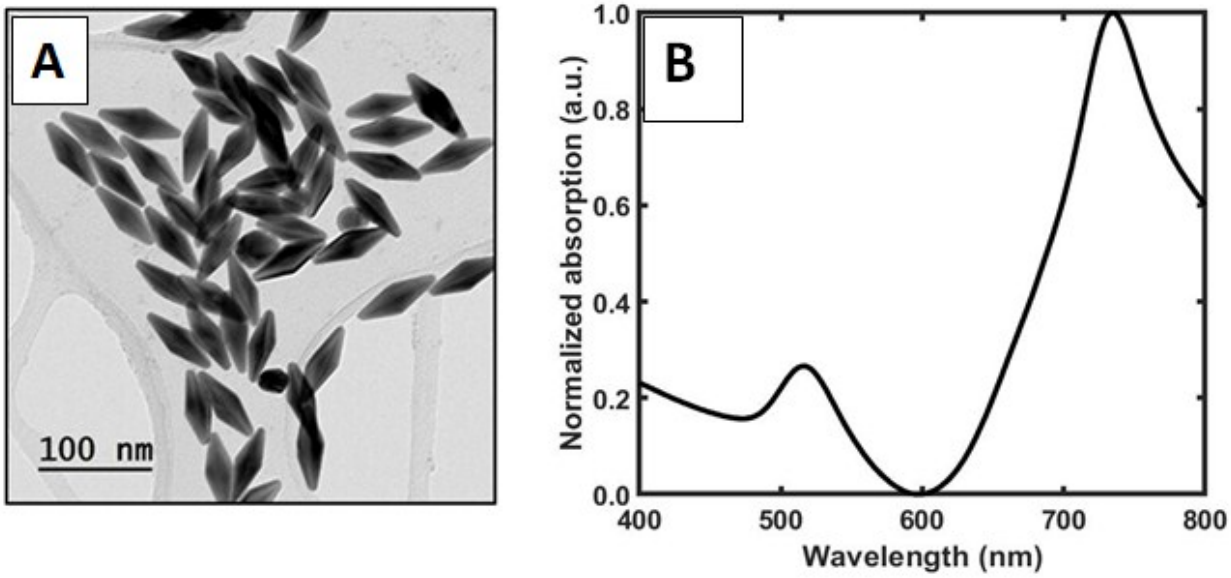

Fig. S1 Characterization of gold bipyramids (AuBPs) used in this study. (A) Scanning electron microscope (SEM) image of AuBPs (B) High energy transverse peak and low energy longitudinal peak of the absorption spectrum of an ensemble AuBPs sample.

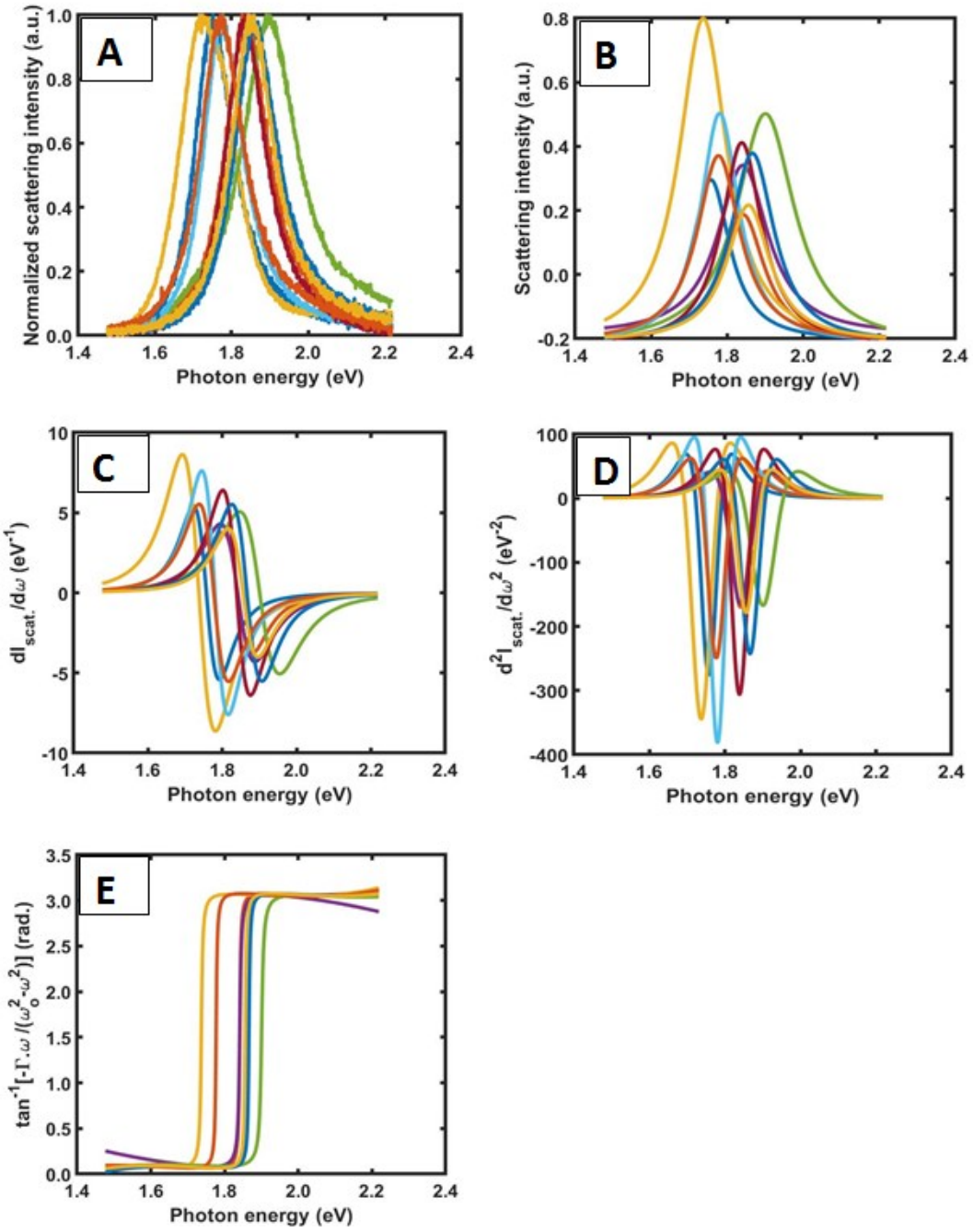

Fig. S2 Plotted data of LSPR of single AuBPs (A) and their fitted curves (B), First (C) and Second (D) derivatives and Scattering phases (E) for air refractive index medium.

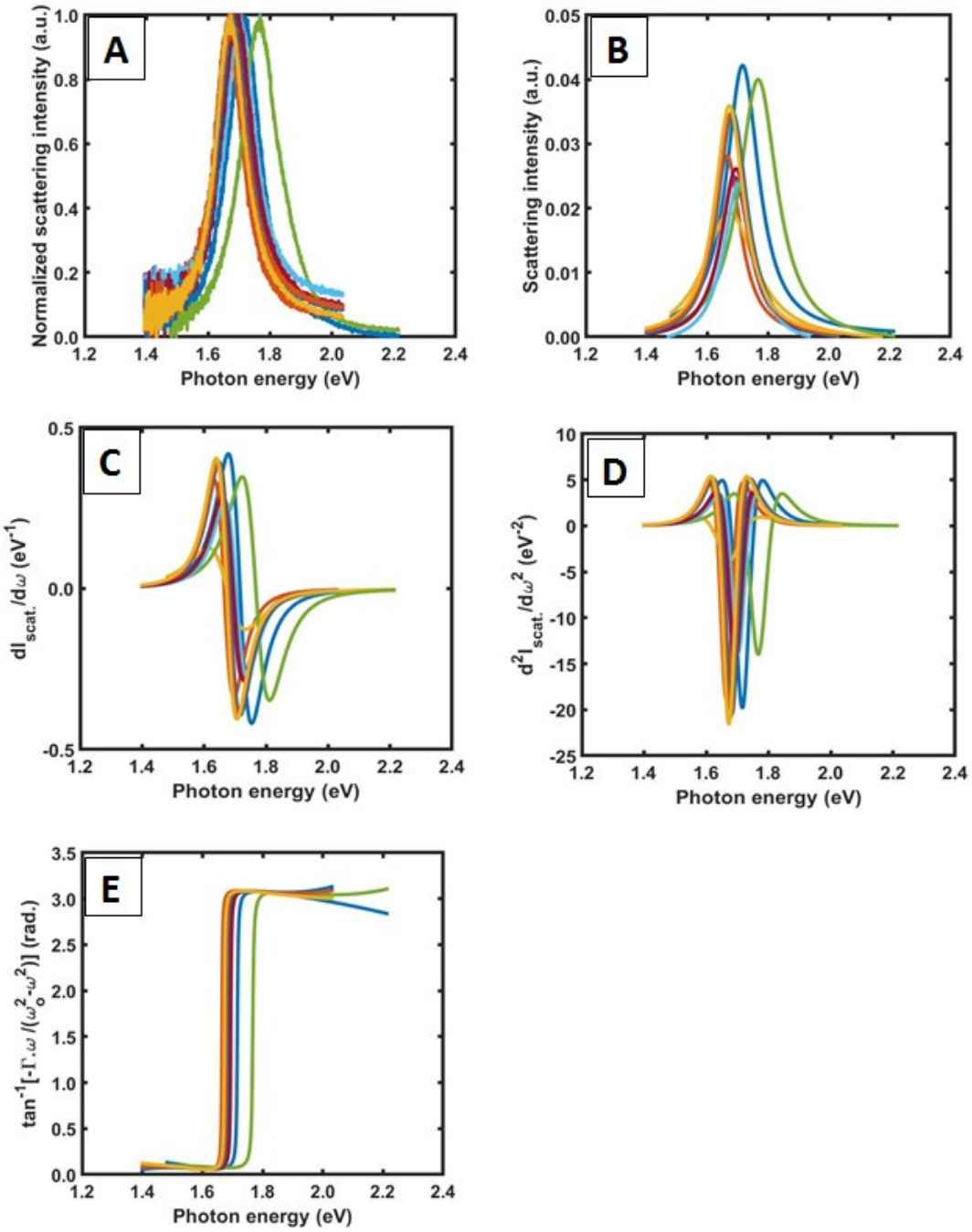

Fig. S3 Plotted data of LSPR of single AuBPs (A) and their fitted curves (B), First (C) and Second (D) derivatives and Scattering phases (E) for water refractive indexes

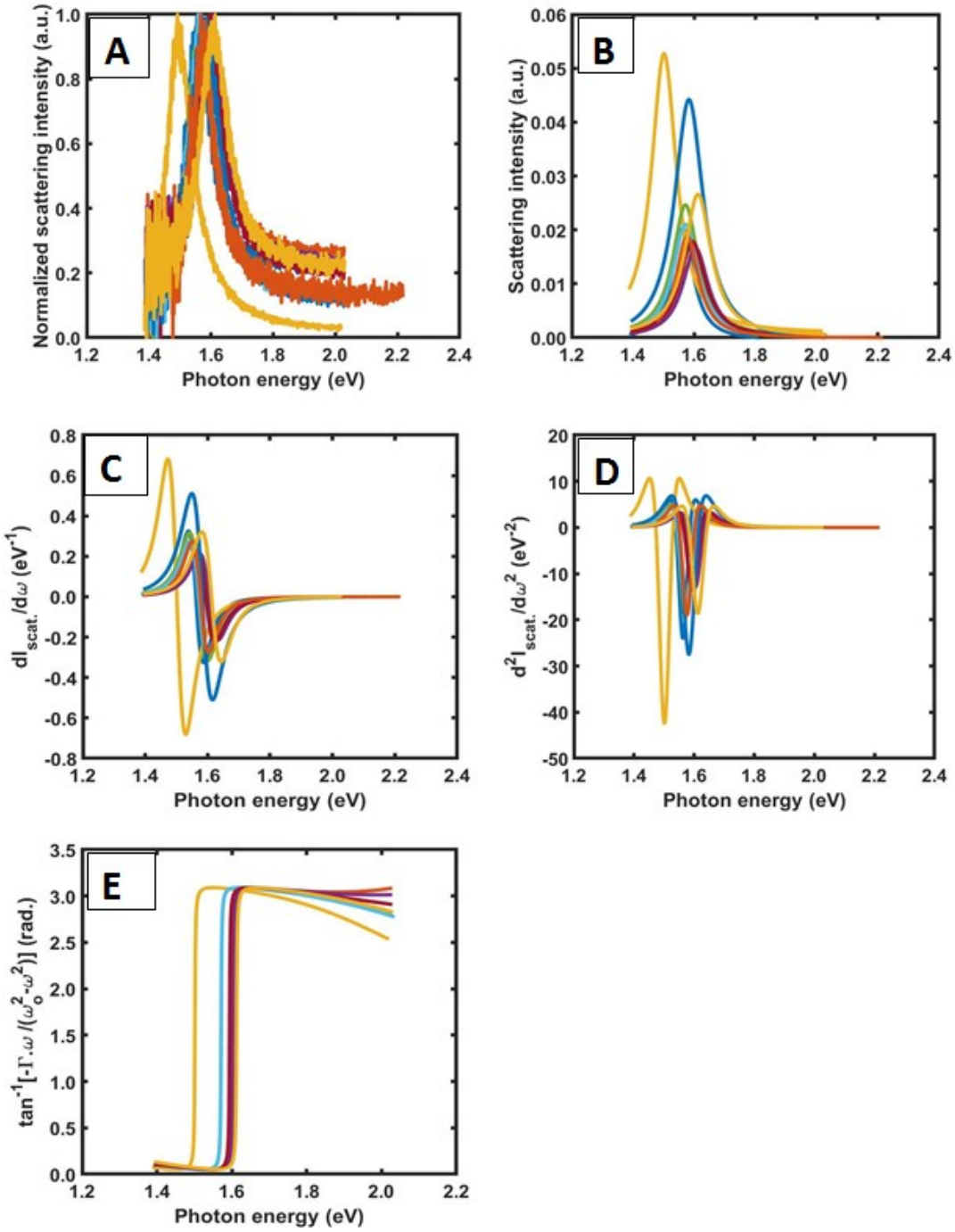

Fig. S4 Plotted data of LSPR of single AuBPs (A) and their fitted curves (B), First (C) and Second (D) derivatives and Scattering phases (E) for oil refractive indexes

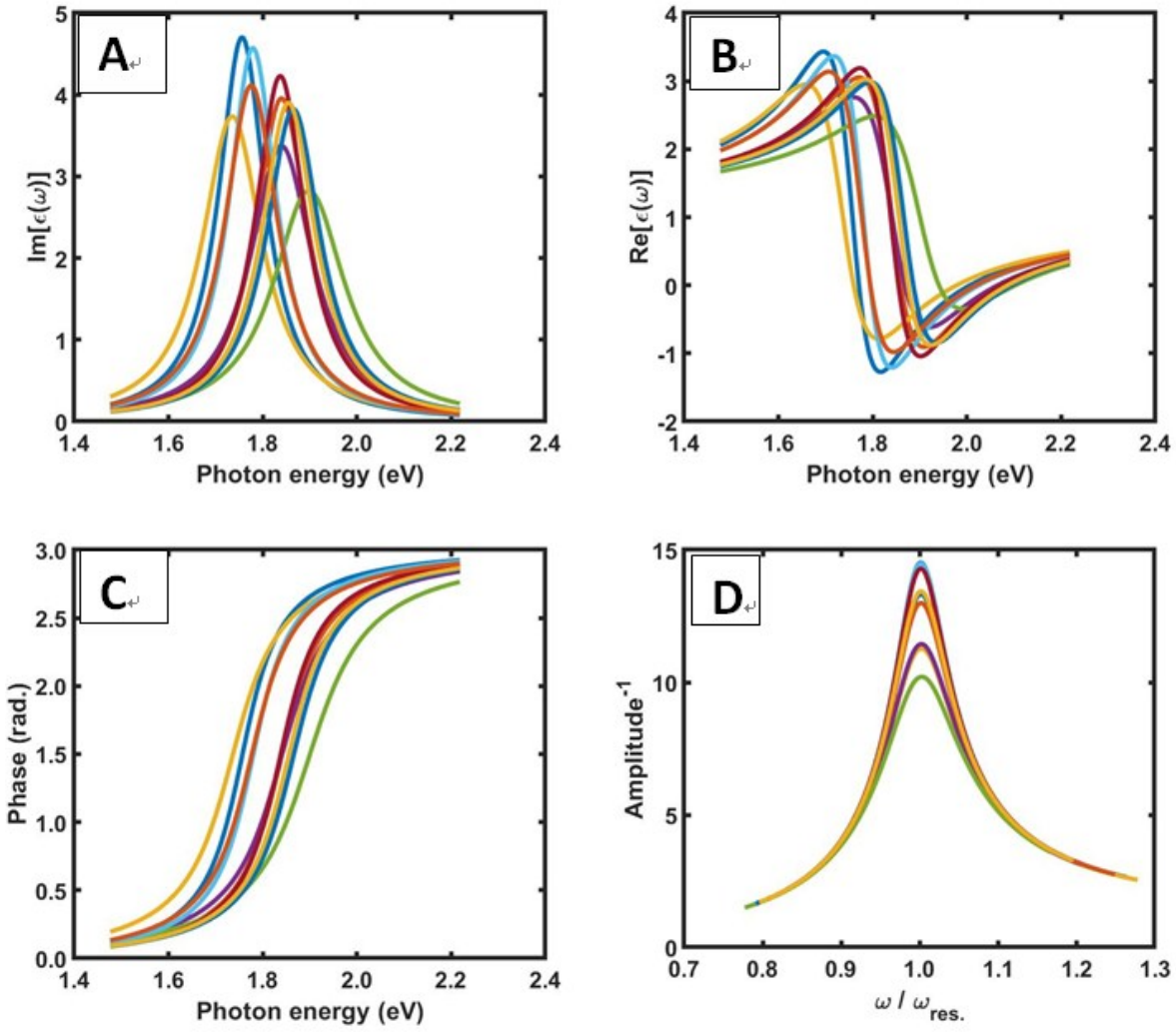

Fig. S5 Plotted data of Im[ε(ω)] (A), Re[ε(ω)] (B), Phase of dipole (C) and Amplitude (D) for changes of complex dielectric functions for air refractive index.

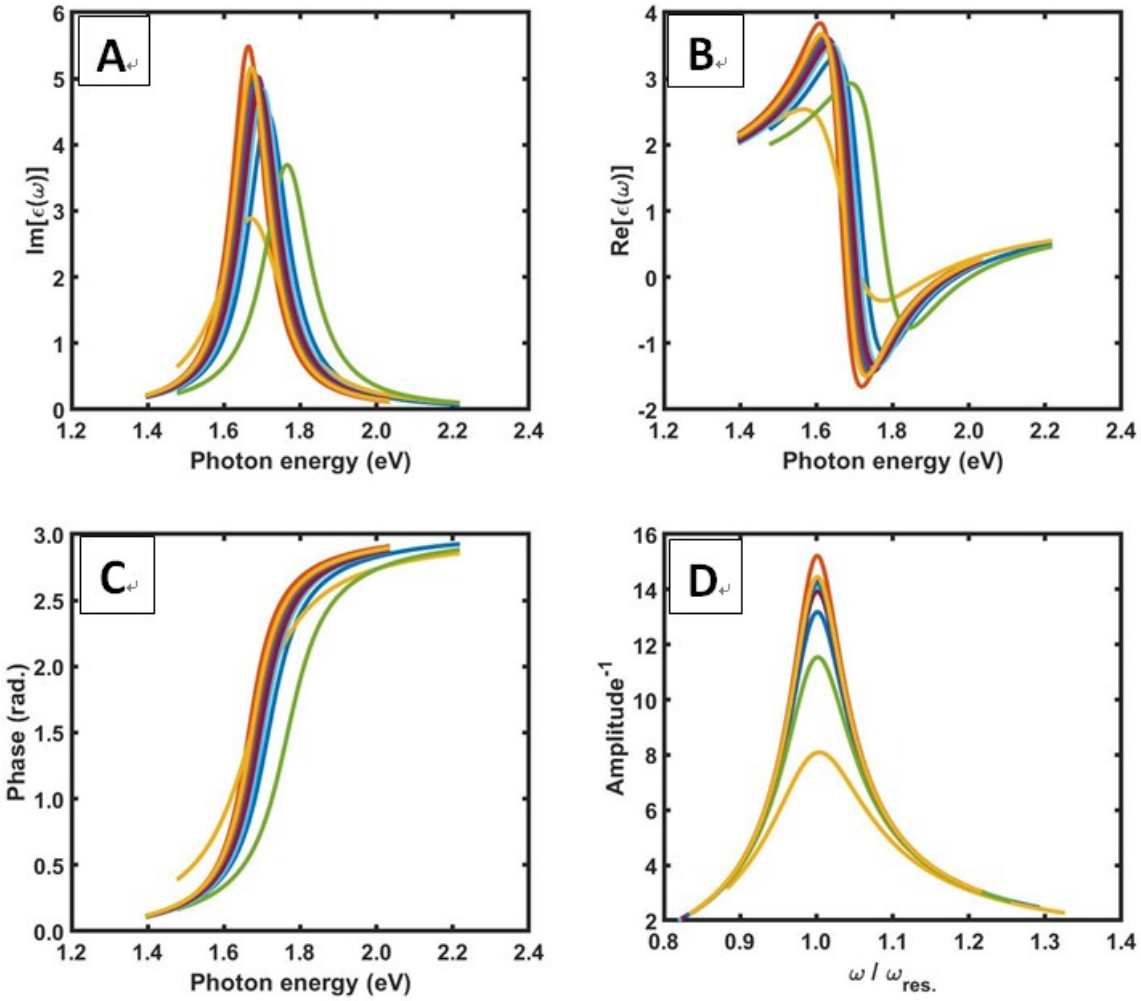

Fig. S6 Plotted data of Im[ε(ω)] (A), Re[ε(ω)] (B), Phase of dipole (C) and Amplitude (D) for changes of complex dielectric functions for water refractive index.

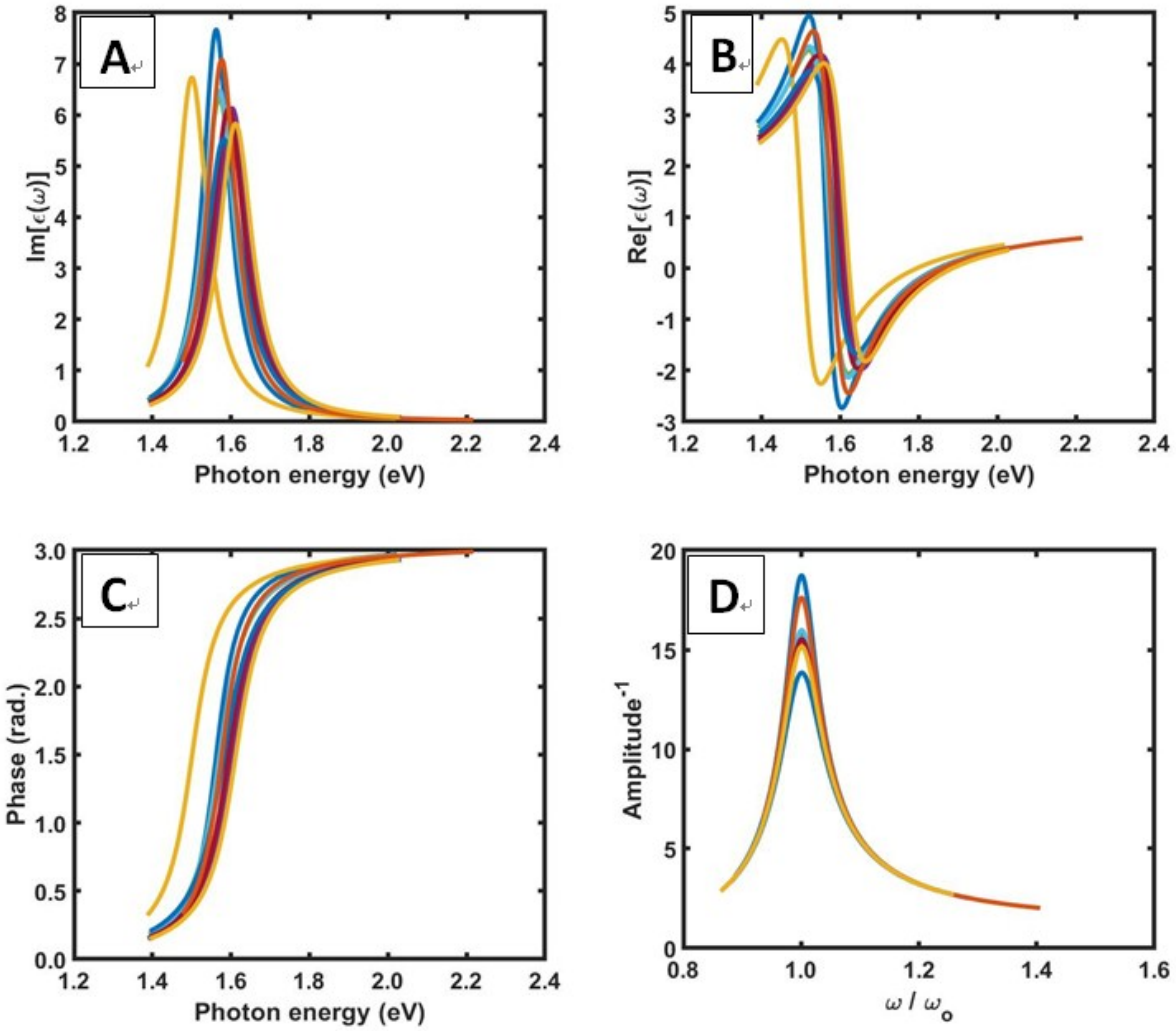

Fig. S7 Plotted data of Im[ε(ω)] (A), Re[ε(ω)] (B), Phase of dipole (C) and Amplitude (D) for changes of complex dielectric functions for oil refractive index.